Electron–hole asymmetry and energy gaps in bilayer graphene

2010 Semicond. Sci. Technol. 25 033001

(http://iopscience.iop.org/0268-1242/25/3/033001)

IOP Publishing Semiconductor Science and Technology

Semicond. Sci. Technol. **25** (2010) 033001 (6pp) doi:10.1088/0268-1242/25/3/033001

TOPICAL REVIEW

Electron–hole asymmetry and energy gaps in bilayer graphene

M Mucha-Kruczyński, E McCann and Vladimir I Fal'ko

Department of Physics, Lancaster University, Lancaster, LA1 4YB, UK

Received 15 April 2009, in final form 13 August 2009
Published 3 February 2010
Online at stacks.iop.org/SST/25/033001

Abstract

We review the tight-binding model of bilayer graphene which describes four low-energy electronic bands near the corner of the first Brillouin zone. The model takes into account terms arising from nearest and next-nearest neighbour hopping within each layer, non-orthogonality of atomic orbitals, various inter-layer couplings, as well as three independent parameters that describe differences between the on-site energies of the four atoms in the unit cell. We generalize the derivation of the two-component effective Hamiltonian that describes the behaviour of chiral quasiparticles at very low energy, taking these terms into account. Then, we explain how the various terms produce features in the electronic band structure, focussing on electron–hole asymmetry and the opening of an energy gap between the conduction and valence bands.

1. Introduction

The isolation of individual graphene flakes a few years ago [1] led to the realization that electrons in graphene are chiral, displaying properties analogous to relativistic fermions including a linear dispersion relation, unusual sequencing of integer quantum Hall effect plateaus [2–4], suppression of backscattering [5, 6] and anisotropic scattering at interfaces [7, 8]. In monolayer graphene, the honeycomb lattice is composed of two triangular sublattices, and wavefunction amplitudes on the sublattices can be written as a pseudospin, analogous to the two components of a spin-1/2 elementary particle. The pseudospin lies in the plane of the graphene layer, and the property of chirality means that its orientation is fixed to be in the same direction as the electron's momentum.

The behaviour of low-energy electrons in bilayer graphene [9, 10] is, perhaps, even more striking than that in monolayers. There is also a pseudospin degree of freedom; in bilayers it is associated with wavefunction amplitudes on the two layers, and electrons are chiral: the pseudospin lies in the plane of the layers and turns twice as quickly as the direction of momentum [11]. From a technological point of view, bilayer graphene holds huge potential because it is a semiconductor with a gate-tuneable band gap between its conduction and valence bands [11–20] as observed in photoemission [10] and transport [21, 22] experiments. Recently, there have been a number of spectroscopic measurements including angle-resolved photoelectron spectroscopy [10, 23], Raman spectroscopy [24–26], cyclotron mass [21], cyclotron resonance [27] and infrared spectroscopy [28–30], determining the electronic band structure of bilayer graphene including observations of electron–hole asymmetry.

The first half of this paper begins, in section 2, with a review of the tight-binding model of bilayer graphene and its use in describing four low-energy electronic bands near the corner of the first Brillouin zone. We take into account a number of terms arising from various inter-atomic couplings as well as three independent parameters U, Δ, Δ_{AB} that describe differences between the on-site energies of the four atoms in the unit cell. Then, in section 3, we include these terms when generalizing the derivation of a two-component effective Hamiltonian [11] that describes the behaviour of chiral quasiparticles at very low energy. This review allows us, in the second half of the paper, to compare how various terms in the model produce features in the low-energy electronic band structure. As described in section 4, two of the on-site asymmetry parameters, U, Δ_{AB}, contribute to the opening of an energy gap, with and without a distinctive 'Mexican hat' structure in the low-energy bands, respectively. The third on-site asymmetry parameter, Δ, contributes to electron–hole asymmetry, as do a number of inter-atomic coupling terms, and, as explained in section 5, this illustrates that different

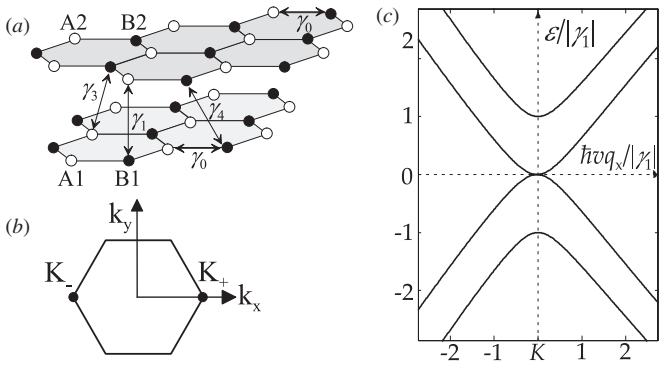

Figure 1. (*a*) Schematic of the bilayer lattice containing four sites in the unit cell: $A1$ (white circles) and $B1$ (black) in the bottom layer, and $A2$ (white) and $B2$ (black) in the top layer. (*b*) Schematic of the hexagonal Brillouin zone with two inequivalent valleys $K_\pm$. (*c*) Low-energy bands in the vicinity of valley K_+ in the absence of lattice asymmetry (where $\mathbf{q}$ is the wave vector measured from the centre of the valley). We use parameter values $\gamma_0 = 3.0$ eV, $\gamma_1 = 0.35$ eV, $\gamma_3 = 0.15$ eV, $\gamma_4 = \gamma_n = 0$ eV, $s_0 = s_1 = 0$, $\Delta_{AB} = \Delta = U = 0$.

microscopic mechanisms may produce the same or similar features, impairing the ability to differentiate between such mechanisms experimentally.

2. The tight-binding model of bilayer graphene

Bilayer graphene [9–11] is composed of two coupled honeycomb lattices of carbon atoms, with inequivalent sites $A1$, $B1$ and $A2$, $B2$ in them. The two layers are arranged according to Bernal ($A2$–$B1$) stacking [11] as shown in figure 1(*a*). It means that half of the sites, $A2$ and $B1$, lie directly above or below a counterpart in the other layer, and they are connected to it by a relatively strong inter-layer coupling γ_1. In order to model the electronic band structure of bilayer graphene, we generalize a standard method [31, 32] to obtain a tight-binding Hamiltonian $\hat{H}$ and an overlap-integral matrix $\hat{S}$ (that takes into account non-orthogonality of orbitals on adjacent atomic sites), $\hat{H}\Psi = \epsilon_{\mathbf{q}}\hat{S}\Psi$. In the space of coefficients $\Psi^T = (\psi_{A1}, \psi_{B2}, \psi_{A2}, \psi_{B1})$ this yields [11, 12, 33–35]

$$\hat{H} = \begin{pmatrix} \epsilon_{A1} - \gamma_n|f(\mathbf{k})|^2 & \gamma_3 f^*(\mathbf{k}) & \gamma_4 f(\mathbf{k}) & -\gamma_0 f(\mathbf{k}) \\ \gamma_3 f(\mathbf{k}) & \epsilon_{B2} - \gamma_n|f(\mathbf{k})|^2 & -\gamma_0 f^*(\mathbf{k}) & \gamma_4 f^*(\mathbf{k}) \\ \gamma_4 f^*(\mathbf{k}) & -\gamma_0 f(\mathbf{k}) & \epsilon_{A2} - \gamma_n|f(\mathbf{k})|^2 & \gamma_1 \\ -\gamma_0 f^*(\mathbf{k}) & \gamma_4 f(\mathbf{k}) & \gamma_1 & \epsilon_{B1} - \gamma_n|f(\mathbf{k})|^2 \end{pmatrix},$$

$$\hat{S} = \begin{pmatrix} 1 & 0 & 0 & s_0 f(\mathbf{k}) \\ 0 & 1 & s_0 f^*(\mathbf{k}) & 0 \\ 0 & s_0 f(\mathbf{k}) & 1 & s_1 \\ s_0 f^*(\mathbf{k}) & 0 & s_1 & 1 \end{pmatrix}, \qquad (1)$$

$$f(\mathbf{k}) = e^{ik_y a/\sqrt{3}} + 2e^{-ik_y a/2\sqrt{3}}\cos(k_x a/2). \qquad (2)$$

In order to parametrize tight-binding couplings relevant to bilayer graphene,[1] we have adapted the notation of the Slonczewski–Weiss–McClure model [36–38] that is often employed to describe bulk graphite. The Hamiltonian equation (1) includes many terms but, roughly speaking, parameters γ_0 and γ_1 determine the most important features of the band structure. The parameter γ_0 describes the strength of nearest-neighbour hopping within each honeycomb layer, yielding the in-plane velocity $v = (\sqrt{3}/2)a\gamma_0/\hbar$ (see footnote 1), where a is the lattice constant and parameter γ_1 describes inter-layer $A2$–$B1$ coupling. There is a degeneracy point at each of two inequivalent corners $\mathbf{K}_\pm = \pm(4\pi/3a, 0)$ of the hexagonal first Brillouin zone, also referred to as valleys, figure 1(*b*). Near the centre of each valley, there are four electronic bands, figure 1(*c*), two in the conduction band and two in the valence band. Of them, two bands, related to electronic orbitals on $A2$ and $B1$ sublattices, are split away from zero energy by about $\pm|\gamma_1|$. Henceforth, they shall be referred to as split bands. The other two bands, formed by orbitals based upon sublattices $A1$ and $B2$, approach each other near zero energy with an approximately parabolic dispersion $\epsilon \approx \pm\hbar^2q^2/2m$ (where $\hbar q$ is the magnitude of the momentum measured from the centre of the valley and the effective mass is $m = \gamma_1/2v^2$) and we shall refer to them as degenerate bands. In our plot of the band structure, figure 1(*c*), we use parameter values $\gamma_0 = 3.0$ eV and $\gamma_1 = 0.35$ eV. A lattice constant value of $a = 2.46$ Å yields in-plane velocity $v = 9.71 \times 10^5$ m s^{-1} and effective mass $m = 0.033m_e$.

The angular dependence of $f(\mathbf{k})$ is called trigonal warping because it leads to a deformation of the form of the Fermi line around the centre of each valley. This deformation increases with an increase of the absolute value of the wave vector. In bilayer graphene, a second cause of trigonal warping is the parameter γ_3 describing direct $A1$–$B2$ inter-layer coupling, leading to an effective velocity $v_3 = -(\sqrt{3}/2)a\gamma_3/\hbar$ [39]. Trigonal warping due to γ_3 becomes particularly relevant at very low energy (of the order of 1 meV) where it leads to a Lifshitz transition: the isoenergetic line about each valley is broken into four pockets [11, 16, 40, 41].

The parameter γ_4 describes $A1$–$A2$ and $B1$–$B2$ inter-layer hopping. As described in more detail in the following subsection, it causes asymmetry between the conduction and valence band. A second possible cause of electron–hole asymmetry is non-orthogonality of atomic orbitals as described by the overlap-integral matrix $\hat{S}$ [31]. In particular, we take into account the parameter $s_0 \ll 1$ describing non-orthogonality of orbitals on the same layer and $s_1 \ll 1$ describing non-orthogonality arising from overlaps between orbitals on different layers. In addition, we include next-nearest neighbour hopping within each layer [42, 43], with strength γ_n, as described by the terms $-\gamma_n|f(\mathbf{k})|^2$ appearing on the diagonal.[2] Other weaker tunnelling processes are neglected.

There are four atomic sites in the unit cell and, in principle, they may be held at different energies $\epsilon_{A1}, \epsilon_{B1}, \epsilon_{A2}$ and ϵ_{B2}. Three parameters are needed to account for differences between them. In defining them, note that some authors

[1] The tight-binding parameters are defined as $\gamma_0 = -\langle\Phi_{A1}|H|\Phi_{B1}\rangle = -\langle\Phi_{A2}|H|\Phi_{B2}\rangle$ where Φ_{A1} is an atomic orbital located on site $A1$, $\gamma_1 = +\langle\Phi_{A2}|H|\Phi_{B1}\rangle$, $\gamma_3 = +\langle\Phi_{A1}|H|\Phi_{B2}\rangle$, and $\gamma_4 = +\langle\Phi_{A1}|H|\Phi_{A2}\rangle = +\langle\Phi_{B1}|H|\Phi_{B2}\rangle$.

[2] Throughout this paper, we neglect a factor of $3\gamma_n$ on the diagonal of the Hamiltonian, arising from next-nearest hopping within each layer, because it only produces a trivial shift of the charge-neutrality point.

[12, 28, 29, 35] employ different definitions of A and B sites. The definitions used here are shown in figure 1(a), whereby $A2$ sites lie directly above $B1$ sites. Then, the three independent parameters we use are $\Delta_{AB} = [(\epsilon_{A1} + \epsilon_{A2}) - (\epsilon_{B1} + \epsilon_{B2})]/2$ to describe the difference between on-site energies of A and B sublattice sites on each layer, $\Delta = [(\epsilon_{A1} + \epsilon_{B2}) - (\epsilon_{B1} + \epsilon_{A2})]/2$ for an energy difference between dimer and non-dimer sites [28, 29, 32, 35] and $U = [(\epsilon_{A1} + \epsilon_{B1}) - (\epsilon_{A2} + \epsilon_{B2})]/2$ for inter-layer asymmetry between the two layers arising from the influence of external gates or a doping effect [10–22]:

$$\begin{aligned}
\epsilon_{A1} &= \frac{U}{2} + \frac{\Delta}{2} + \frac{\Delta_{AB}}{2},\\
\epsilon_{B1} &= \frac{U}{2} - \frac{\Delta}{2} - \frac{\Delta_{AB}}{2},\\
\epsilon_{A2} &= -\frac{U}{2} - \frac{\Delta}{2} + \frac{\Delta_{AB}}{2},\\
\epsilon_{B2} &= -\frac{U}{2} + \frac{\Delta}{2} - \frac{\Delta_{AB}}{2}.
\end{aligned} \tag{3}$$

The three asymmetry parameters U, Δ, Δ_{AB} are enough to describe on-site energy differences between the four atoms, but their choice is not unique. For example, the presence of a substrate may lead to a difference between on-site energies of adjacent atoms in the bottom layer $\epsilon_{A1} - \epsilon_{B1} \equiv \Delta + \Delta_{AB}$ [34], leading to both electron–hole asymmetry (arising from Δ) and an energy gap (from Δ_{AB}).

3. The effective low-energy Hamiltonian

There are two independent valleys denoted by K_ξ, where $\xi = \pm 1$ is a valley index, with wave vector $\mathbf{K}_\xi = \xi(4\pi/3a, 0)$ corresponding to the corner of the first Brillouin zone, figure 1(b). In their vicinity, two energy bands, related to electronic orbitals on $A2$ and $B1$ sublattices, are split away from zero energy by about $\pm|\gamma_1|$. The other two bands, formed by orbitals based upon sublattices $A1$ and $B2$, approach each other near zero energy with an approximately parabolic dispersion. Often, it is convenient to use a two-component Hamiltonian describing electrons in these degenerate bands. It was derived in [11] using Green's functions. Alternatively (and equivalently), it is possible to view the eigenvalue equation of the four-component Hamiltonian equation (1) as producing four simultaneous equations for components $\psi_{A1}, \psi_{B2}, \psi_{A2}, \psi_{B1}$. Then, the two-component Hamiltonian can be obtained by eliminating the dimer state components ψ_{A2}, ψ_{B1} by substitution and treating γ_1 as a large energy.

For simplicity, it is common to express the wave vector $\mathbf{k} = \mathbf{K}_\xi + \mathbf{q}$ in terms of the wave vector $\mathbf{q}$ measured from the centre of the valley K_ξ, and to expand the function $f(\mathbf{k})$, equation (2), in terms of $\mathbf{q} = (q_x, q_y)$ for electronic energies much less than the π-band width ($qa \ll 1$):

$$f(\mathbf{k}) \approx -\frac{\sqrt{3}a}{2}(\xi q_x - \mathrm{i}q_y) + \frac{a^2}{8}(\xi q_x + \mathrm{i}q_y)^2. \tag{4}$$

Note that a represents the lattice constant, not the atomic separation (the latter is equal to $a/\sqrt{3}$). Here, we generalize this procedure [11] to include the parameters contained in the four-component Hamiltonian equation (1) to obtain the two-component Hamiltonian describing effective hopping between the $A1$–$B2$ sites.

$$\begin{aligned}
\hat{H}_2 &= \hat{h}_0 + \hat{h}_w + \hat{h}_4 + \hat{h}_n + \hat{h}_U + \hat{h}_\Delta + \hat{h}_{AB},\\
\hat{h}_0 &= -\frac{1}{2m}\begin{pmatrix} 0 & (\pi^\dagger)^2 \\ \pi^2 & 0 \end{pmatrix},\\
\hat{h}_w &= v_3\begin{pmatrix} 0 & \pi \\ \pi^\dagger & 0 \end{pmatrix} + \frac{v_3^2}{6\gamma_3}\begin{pmatrix} 0 & (\pi^\dagger)^2 \\ \pi^2 & 0 \end{pmatrix},\\
\hat{h}_4 &= \frac{2\gamma_4\hbar^2v^2q^2}{\gamma_0\gamma_1}\begin{pmatrix} 1 & 0 \\ 0 & 1 \end{pmatrix},\\
\hat{h}_n &= -\frac{\gamma_n\hbar^2v^2q^2}{\gamma_0^2}\begin{pmatrix} 1 & 0 \\ 0 & 1 \end{pmatrix},\\
\hat{h}_U &= U\left(\frac{1}{2} - \frac{\hbar^2v^2q^2}{\gamma_1^2}\right)\begin{pmatrix} 1 & 0 \\ 0 & -1 \end{pmatrix},\\
\hat{h}_\Delta &= \Delta\left(\frac{1}{2} - \frac{\hbar^2v^2q^2}{\gamma_1^2}\right)\begin{pmatrix} 1 & 0 \\ 0 & 1 \end{pmatrix},\\
\hat{h}_{AB} &= \frac{\Delta_{AB}}{2}\begin{pmatrix} 1 & 0 \\ 0 & -1 \end{pmatrix}
\end{aligned} \tag{5}$$

where the complex momentum operator is $\pi = \xi\hbar q_x + \mathrm{i}\hbar q_y$. The effective Hamiltonian $\hat{H}_2$ determines components (ψ_{A1}, ψ_{B2}) and it is applicable when the intra-layer hopping γ_0 and the inter-layer coupling γ_1 dominate: $|\epsilon|, \hbar vq, |\gamma_3|, |\gamma_4|, |\gamma_n|, |U|, |\Delta|, |\Delta_{AB}| \ll \gamma_0, \gamma_1$. We kept only linear terms in the small parameters $|\gamma_3|, |\gamma_4|, |\gamma_n|, |U|, |\Delta|, |\Delta_{AB}|$ and quadratic in momentum. Terms containing s_0 and s_1 have been neglected since we assume that $|s_0|, |s_1| \ll 1$.

The first term, $\hat{h}_0$, takes into account $A1B2$ hopping via the $A2B1$ dimer state with effective mass $m = \gamma_1/2v^2$ reflecting the energetic cost γ_1 of a transition via the dimer state. This term in $\hat{H}_2$ yields a parabolic spectrum $\epsilon = \pm\hbar^2q^2/2m$ and quasiparticles described by it are chiral, with a degree of chirality related to Berry phase 2π [11]. The second term $\hat{h}_w$ in the Hamiltonian equation (5) describes weak direct $A1B2$ coupling, leading to the effective velocity $v_3 = -(\sqrt{3}/2)a\gamma_3/\hbar$, where $v_3 \ll v$. In a similar way to bulk graphite [32], the effect of coupling γ_3 is to produce trigonal warping, which becomes particularly relevant at very low energy (of the order of 1 meV) where it leads to a Lifshitz transition [11, 16, 40, 41].

The terms $\hat{h}_4$, $\hat{h}_n$ and $\hat{h}_\Delta$ in equation (5) are proportional to the unit matrix in the lattice subspace of (ψ_{A1}, ψ_{B2}) and, as described in section 5, they contribute to electron–hole asymmetry in the band structure (see footnote 2). By way of contrast, terms $\hat{h}_U$ and $\hat{h}_{AB}$ are proportional to σ_z and thus break the symmetry of the lattice subspace leading to the opening of a gap in the low-energy spectrum.

4. Comparison of gap opening due to inter- and intra-layer asymmetry

As described in section 2, we use three parameters U, Δ and Δ_{AB} to take into account differences between the on-site

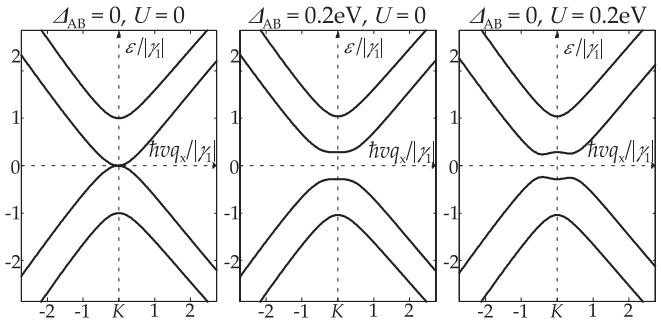

Figure 2. The band structure of bilayer graphene in the vicinity of valley K_+ for no lattice asymmetry (left), finite AB lattice asymmetry Δ_{AB} (centre) or finite inter-layer asymmetry U (right). For clarity, we use large values of asymmetry. Other parameter values are $\gamma_0 = 3.0$ eV, $\gamma_1 = 0.35$ eV, $\gamma_3 = 0.15$ eV, $\gamma_4 = \gamma_n = 0$ eV and $s_0 = s_1 = 0$.

energies of the four sites in the unit cell of bilayer graphene. The parameter Δ does not open a gap, but contributes to electron–hole asymmetry as discussed in section 5, whereas U and Δ_{AB} both contribute to the opening of a gap between the conduction and valence bands. Figure 2 shows the band structure for no lattice asymmetry (left), finite Δ_{AB} (centre) and finite U (right).

The parameter $U = [(\epsilon_{A1} + \epsilon_{B1}) - (\epsilon_{A2} + \epsilon_{B2})]/2$ models inter-layer asymmetry between the two layers arising from external gates or a doping effect [10–22]. The four-component Hamiltonian equation (1), simplified by setting $\Delta_{AB} = \Delta = \gamma_3 = \gamma_4 = \gamma_n = s_0 = s_1 = 0$, yields four valley-degenerate energy bands ϵ_α,

$$\epsilon_\alpha^2 = \frac{\gamma_1^2}{2} + \frac{U^2}{4} + \gamma_0^2 |f(\mathbf{k})|^2 + (-1)^\alpha \sqrt{\frac{\gamma_1^4}{4} + \gamma_0^2 |f(\mathbf{k})|^2 \left(\gamma_1^2 + U^2\right)},$$

where the parameter $\alpha = 2$ for the split bands and $\alpha = 1$ for the degenerate bands [11]. For small wave vector $\mathbf{q}$ in the vicinity of a valley, we may approximate $\gamma_0^2 |f(\mathbf{k})|^2 \approx \hbar^2 v^2 q^2$, equation (4). The appearance of U in the square root leads to a distinctive 'Mexican hat' structure [11, 12] of the degenerate bands ($\alpha = 1$) as shown in figure 2 (right). The parameter U should be tuneable in bilayer graphene, and its dependence on externally applied gate voltage has been calculated taking into account screening effects in both bilayer [13–15, 20, 21] and multilayer graphene [44–46].

The parameter $\Delta_{AB} = [(\epsilon_{A1} + \epsilon_{A2}) - (\epsilon_{B1} + \epsilon_{B2})]/2$ is used to describe intra-layer asymmetry, i.e. a difference between on-site energies of A and B sublattice sites on each layer. In this case, the four-component Hamiltonian equation (1), simplified by setting $U = \Delta = \gamma_3 = \gamma_4 = \gamma_n = s_0 = s_1 = 0$ gives

$$\epsilon_\alpha^2 = \frac{\Delta_{AB}^2}{4} + \frac{\gamma_1^2}{4}\left[\sqrt{1 + \frac{4\gamma_0^2 |f(\mathbf{k})|^2}{\gamma_1^2}} + (-1)^\alpha\right]^2.$$

The effect of Δ_{AB} on the band structure is to open a gap by a more or less trivial shift of the energy as shown in figure 2 (centre). Unlike parameter U, it does not lead to a Mexican hat structure and so, in principle, it should be possible to differentiate the presence of finite U from that of finite Δ_{AB}.

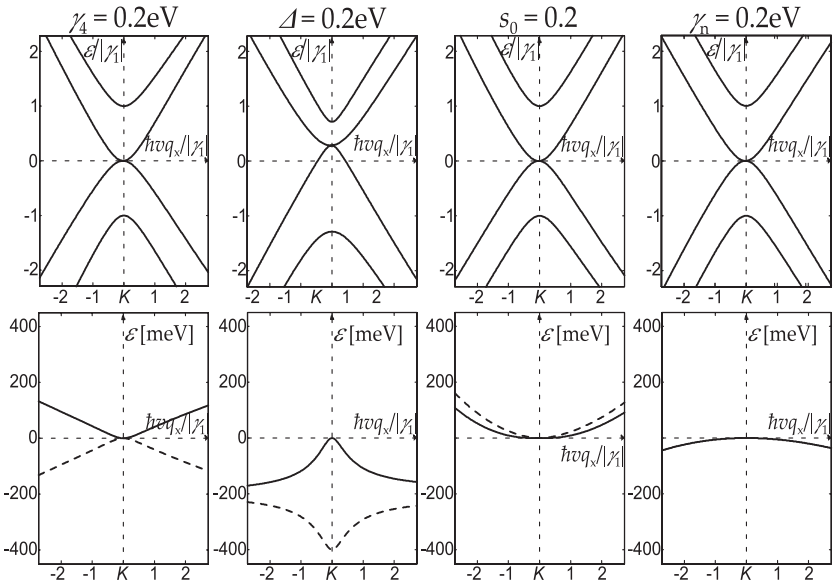

Figure 3. Top row: the band structure of bilayer graphene in the vicinity of valley K_+ comparing different parameters that contribute to electron–hole asymmetry. From left to right, $\gamma_4 = 0.2$ eV, $\Delta = 0.2$ eV, $s_0 = 0.2$ and $\gamma_n = 0.2$ eV. These values are taken for illustrative purposes. Other parameter values are $\gamma_0 = 3.0$ eV, $\gamma_1 = 0.35$ eV, $\gamma_3 = 0.15$ eV and $s_1 = 0$. Bottom row: asymmetry $|\epsilon_c| - |\epsilon_v|$ between the energies ϵ_c and ϵ_v of the degenerate conduction and valence bands (solid) or the split bands (dashed) for the same parameters as in the top row, with energies measured with respect to the touching point of the degenerate bands at the centre of the valley. In the plot on the bottom right, for $\gamma_n = 0.2$ eV, solid and dashed lines lie on top of each other.

5. Electron–hole asymmetry in the band structure

In this section, we will compare four possible causes of electron–hole asymmetry that appear in Hamiltonian equation (1), namely, the inter-layer coupling parameter γ_4, parameter $\Delta = [(\epsilon_{A1} + \epsilon_{B2}) - (\epsilon_{B1} + \epsilon_{A2})]/2$ that takes into account a possible energy difference between dimer and non-dimer sites [28, 29, 32, 35], parameter s_0 describing non-orthogonality of adjacent atomic orbitals on each layer [31] and next-nearest neighbour hopping γ_n within each layer [42, 43]. The electronic band structure calculated without taking these parameters into account is shown in figure 1(*c*). Taking each of the four parameters into account in turn, while neglecting the other three, results in the band structures plotted in the top row of figure 3. In order to illustrate the nature of electron–hole asymmetry, the bottom row of figure 3 shows the asymmetry between the conduction and valence bands $|\epsilon_c| - |\epsilon_v|$ of the degenerate bands (solid) and the split bands (dashed). The asymmetry is calculated by treating the touching point of the degenerate bands (at the centre of the valley, $q = 0$) as the zero of energy. Thus, by definition, each solid curve displays zero asymmetry at $q_x = 0$.

The bottom row of figure 3 shows that parameters γ_4, Δ, s_0 and γ_n all contribute to electron–hole asymmetry (in figure 3, arbitrary values of these parameters are used for illustrative purposes). As pointed out in [29], it is possible to distinguish the influence of γ_4 and Δ by comparing the asymmetry between the degenerate bands (solid lines) with the asymmetry between the split bands (dashed). Specifically, Δ produces a non-zero value of the asymmetry between the split bands (dashed) even at the centre of the valley. For γ_4, the sign of the asymmetry between the degenerate bands (solid lines) and that between the split bands (dashed) is different, but in both cases the asymmetry has an almost linear dependence on momentum. The plots in figure 3 for finite s_0 and γ_n suggest that it should be difficult to differentiate between asymmetry caused by non-orthogonality of orbitals and next-nearest neighbour hopping.

6. Conclusions

The first half of this paper reviewed the use of the tight-binding model to describe four low-energy electronic bands near the corner of the first Brillouin zone of bilayer graphene. The model takes into account terms arising from nearest- and next-nearest neighbour hopping within each layer, non-orthogonality of atomic orbitals, various inter-layer couplings, as well as three independent parameters U, Δ, Δ_{AB} that describe differences between the on-site energies of the four atoms in the unit cell. In the second half of the paper, we demonstrated that there are a number of different microscopic mechanisms that may contribute, at least in principle, to electron–hole asymmetry in the low-energy band structure of bilayer graphene. Examples include inter-layer coupling γ_4, an energy difference Δ between dimer and non-dimer sites in the unit cell [28, 29, 32, 35], next-nearest neighbour hopping within each graphene layer [42, 43] and non-orthogonality between atomic orbitals [31]. With care, it may be possible to differentiate between some of them experimentally. Likewise, there are two independent parameters describing energy differences between sites in the unit cell that contribute to the opening of a gap between the conduction and valence bands: inter-layer asymmetry U and intra-layer asymmetry Δ_{AB} (between A and B sublattice sites on each layer). Again, in principle it could be possible to distinguish between them as U leads to a Mexican hat band structure [11, 12] whereas Δ_{AB} does not. In our analysis, when comparing the conduction and valence bands, we assumed that the tight-binding parameters remain constant during such a comparison. However, one could imagine a scenario where they would vary during the course of a spectroscopy experiment. For example, the inter-layer asymmetry U is sensitive to the electrostatic environment and it will, in general, vary as the Fermi level in the system is changed. This effect should be taken into account when attempting to measure electron–hole asymmetry experimentally.

Acknowledgments

This project has been funded by EPSRC Portfolio Partnership EP/C511743/1, and EPSRC First Grant EP/E063519/1, ESF FoNE project SpiCo EP/D062918/1, the Royal Society, and the Daiwa Anglo-Japanese Foundation.

References

[1] Novoselov K S, Geim A K, Morozov S V, Jiang D, Zhang Y, Dubonos S V, Grigorieva I V and Firsov A A 2004 *Science* **306** 666
[2] Novoselov K S, Geim A K, Morozov S V, Jiang D, Katsnelson M I, Grigorieva I V, Dubonos S V and Firsov A A 2005 *Nature* **438** 197
[3] Zhang Y, Tan Y W, Stormer H L and Kim P 2005 *Nature* **438** 201
[4] Geim A K and Novoselov K S 2007 *Nature Mater.* **6** 183
[5] Ando T, Nakanishi T and Saito R 1998 *J. Phys. Soc. Japan.* **67** 2857
[6] McEuen P L, Bockrath M, Cobden D H, Yoon Y G and Louie S G 1999 *Phys. Rev. Lett.* **83** 5098
[7] Katsnelson M I, Novoselov K S and Geim A K 2006 *Nature Phys.* **2** 620
[8] Cheianov V V and Fal'ko V I 2006 *Phys. Rev.* B **74** 041403(R)
[9] Novoselov K S, McCann E, Morozov S V, Fal'ko V I, Katsnelson M I, Zeitler U, Jiang D, Schedin F and Geim A K 2006 *Nature Phys.* **2** 177
[10] Ohta T, Bostwick A, Seyller T, Horn K and Rotenberg E 2006 *Science* **313** 951
[11] McCann E and Fal'ko V I 2006 *Phys. Rev. Lett.* **96** 086805
[12] Guinea F, Castro Neto A H and Peres N M R 2006 *Phys. Rev.* B **73** 245426
[13] McCann E 2006 *Phys. Rev.* B **74** 161403(R)
[14] Min H, Sahu B R, Banerjee S K and MacDonald A H 2007 *Phys. Rev.* B **75** 155115
[15] Aoki M and Amawashi H 2007 *Solid State Commun.* **142** 123
[16] McCann E, Abergel D S L and Fal'ko V I 2007 *Solid State Commun.* **143** 110

[17] Guinea F, Castro Neto A H and Peres N M R 2007 *Solid State Commun.* **143** 116
[18] McCann E, Abergel D S L and Fal'ko V I 2007 *Eur. Phys. J. Spec. Top.* **148** 15
[19] Guinea F, Castro Neto A H and Peres N M R 2007 *Eur. Phys. J. Spec. Top.* **148** 117
[20] Gava P, Lazzeri M, Saitta A M and Mauri F 2009 *Phys. Rev.* B **79** 165431
[21] Castro E V, Novoselov K S, Morozov S V, Peres N M R, Lopes dos Santos J M B, Nilsson J, Guinea F, Geim A K and Castro Neto A H 2007 *Phys. Rev. Lett.* **99** 216802
[22] Oostinga J B, Heersche H B, Liu X, Morpurgo A F and Vandersypen L M K 2007 *Nature Mater.* **7** 151
[23] Ohta T, Bostwick A, McChesney J L, Seyller T, Horn K and Rotenberg E 2007 *Phys. Rev. Lett.* **98** 206802
[24] Ferrari A C *et al* 2006 *Phys. Rev. Lett.* **97** 187401
[25] Malard L M, Nilsson J, Elias D C, Brant J C, Plentz F, Alves E S, Castro Neto A H and Pimenta M A 2007 *Phys. Rev.* B **76** 201401(R)
[26] Das A, Chakraborty B, Piscanec S, Pisana S, Sood A K and Ferrari A C 2009 *Phys. Rev.* B **79** 155417
[27] Henriksen E A, Jiang Z, Tung L-C, Schwartz M E, Takita M, Wang Y-J, Kim P and Stormer H L 2008 *Phys. Rev. Lett.* **100** 087403
[28] Li Z Q, Henriksen E A, Jiang Z, Hao Z, Martin M C, Kim P, Stormer H L and Basov D N 2009 *Phys. Rev. Lett.* **102** 037403
[29] Zhang L M, Li Z Q, Basov D N, Fogler M M, Hao Z and Martin M C 2008 *Phys. Rev.* B **78** 235408
[30] Kuzmenko A B, van Heumen E, van der Marel D, Lerch P, Blake P, Novoselov K S and Geim A K 2009 *Phys. Rev.* B **79** 115441
[31] Saito R, Dresselhaus G and Dresselhaus M S 1998 *Physical Properties of Carbon Nanotubes* (London: Imperial College Press)
[32] Dresselhaus M S and Dresselhaus G 2002 *Adv. Phys.* **51** 1
[33] Partoens B and Peeters F M 2006 *Phys. Rev.* B **74** 075404
[34] Mucha-Kruczyński M, Tsyplyatyev O, Grishin A, McCann E, Fal'ko V I, Bostwick A and Rotenberg E 2008 *Phys. Rev.* B **77** 195403
[35] Nilsson J, Castro Neto A H, Guinea F and Peres N M R 2008 *Phys. Rev.* B **78** 045405
[36] Slonczewski J C and Weiss P R 1958 *Phys. Rev.* **109** 272
[37] McClure J W 1957 *Phys. Rev.* **108** 612
[38] McClure J W 1960 *Phys. Rev.* **119** 606
[39] Kechedzhi K, Fal'ko V I, McCann E and Altshuler B L 2007 *Phys. Rev. Lett.* **98** 176806
[40] Koshino M and Ando T 2006 *Phys. Rev.* B **73** 245403
[41] Cserti J, Csordás A and Dávid G 2007 *Phys. Rev. Lett.* **99** 066802
[42] Sasaki K, Murakami S and Saito R 2006 *Appl. Phys. Lett.* **88** 113110
[43] Peres N M R, Guinea F and Castro Neto A H 2006 *Phys. Rev.* B **73** 125411
[44] Guinea F 2007 *Phys. Rev.* B **75** 235433
[45] Koshino M and McCann E 2009 *Phys. Rev.* B **79** 125443
[46] Avetisyan A A, Partoens B and Peeters F M 2009 *Phys. Rev.* B **79** 035421